

**System-size dependence of open-heavy-flavor production in nucleus-nucleus collisions
at $\sqrt{s_{NN}}=200$ GeV**

- A. Adare,¹¹ S. Afanasiev,²⁷ C. Aidala,^{12,38} N.N. Ajitanand,⁵⁵ Y. Akiba,^{49,50} H. Al-Bataineh,⁴³ J. Alexander,⁵⁵ K. Aoki,^{31,49} N. Apadula,⁵⁶ L. Aphecetche,⁵⁷ R. Armendariz,⁴³ S.H. Aronson,⁶ J. Asai,⁵⁰ E.T. Atomssa,³² R. Averbeck,⁵⁶ T.C. Awes,⁴⁵ B. Azmoun,⁶ V. Babintsev,²¹ G. Baksay,¹⁷ L. Baksay,¹⁷ A. Baldissieri,¹⁴ K.N. Barish,⁷ P.D. Barnes,^{35,*} B. Bassalleck,⁴² S. Bathe,^{4,7} S. Batsouli,⁴⁵ V. Baublis,⁴⁸ S. Baumgart,⁴⁹ A. Bazilevsky,⁶ S. Belikov,^{6,*} R. Bennett,⁵⁶ Y. Berdnikov,⁵² A.A. Bickley,¹¹ J.G. Boissevain,³⁵ H. Borel,¹⁴ K. Boyle,⁵⁶ M.L. Brooks,³⁵ H. Buesching,⁶ V. Bumazhnov,²¹ G. Bunce,^{6,50} S. Butsyk,^{35,56} S. Campbell,⁵⁶ B.S. Chang,⁶⁵ J.-L. Charvet,¹⁴ S. Chernichenko,²¹ C.Y. Chi,¹² J. Chiba,²⁸ M. Chiu,²² I.J. Choi,⁶⁵ T. Chujo,⁶¹ P. Chung,⁵⁵ A. Churnyn,²¹ V. Cianciolo,⁴⁵ C.R. Clevon,¹⁹ B.A. Cole,¹² M.P. Comets,⁴⁶ P. Constantin,³⁵ M. Csanád,¹⁶ T. Csörgő,⁶⁴ T. Dahms,⁵⁶ K. Das,¹⁸ G. David,⁶ M.B. Deaton,¹ K. Dehmelt,¹⁷ H. Delagrangé,⁵⁷ A. Denisov,²¹ D. d'Enterria,¹² A. Deshpande,^{50,56} E.J. Desmond,⁶ O. Dietzsch,⁵³ A. Dion,⁵⁶ M. Donadelli,⁵³ O. Drapier,³² A. Drees,⁵⁶ A.K. Dubey,⁶³ J.M. Durham,³⁵ A. Durum,²¹ V. Dzhordzhadze,⁷ Y.V. Efremenko,⁴⁵ J. Egdemir,⁵⁶ F. Ellinghaus,¹¹ W.S. Emam,⁷ A. Enokizono,³⁴ H. En'yo,^{49,50} S. Esumi,⁶⁰ K.O. Eyser,⁷ D.E. Fields,^{42,50} M. Finger,^{8,27} M. Finger, Jr.,^{8,27} F. Fleuret,³² S.L. Fokin,³⁰ Z. Fraenkel,^{63,*} J.E. Frantz,^{44,56} A. Franz,⁶ A.D. Frawley,¹⁸ K. Fujiwara,⁴⁹ Y. Fukao,^{31,49} T. Fusayasu,⁴¹ S. Gadrat,³⁶ I. Garishvili,⁵⁸ A. Glenn,¹¹ H. Gong,⁵⁶ M. Gonin,³² J. Gosset,¹⁴ Y. Goto,^{49,50} R. Granier de Cassagnac,³² N. Grau,^{2,25} S.V. Greene,⁶¹ M. Grosse Perdekamp,^{22,50} T. Gunji,¹⁰ H.-Å. Gustafsson,^{37,*} T. Hachiya,²⁰ A. Hadj Henni,⁵⁷ C. Haegemann,⁴² J.S. Haggerty,⁶ H. Hamagaki,¹⁰ R. Han,⁴⁷ H. Harada,²⁰ E.P. Hartouni,³⁴ K. Haruna,²⁰ E. Haslum,³⁷ R. Hayano,¹⁰ X. He,¹⁹ M. Heffner,³⁴ T.K. Hemmick,⁵⁶ T. Hester,⁷ H. Hiejima,²² J.C. Hill,²⁵ R. Hobbs,⁴² M. Hohlmann,¹⁷ W. Holzmann,⁵⁵ K. Homma,²⁰ B. Hong,²⁹ T. Horaguchi,^{49,59} D. Hornback,⁵⁸ T. Ichihara,^{49,50} H. Inuma,^{31,49} K. Imai,^{26,31,49} M. Inaba,⁶⁰ Y. Inoue,^{49,51} D. Isenhower,¹ L. Isenhower,¹ M. Ishihara,⁴⁹ T. Isobe,¹⁰ M. Issah,⁵⁵ A. Isupov,²⁷ B.V. Jacak,⁵⁶ J. Jia,¹² J. Jin,¹² O. Jinnouchi,⁵⁰ B.M. Johnson,⁶ K.S. Joo,⁴⁰ D. Jouan,⁴⁶ F. Kajihara,¹⁰ S. Kametani,^{10,62} N. Kamihara,⁴⁹ J. Kamin,⁵⁶ M. Kaneta,⁵⁰ J.H. Kang,⁶⁵ H. Kanou,^{49,59} D. Kawall,⁵⁰ A.V. Kazantsev,³⁰ A. Khanzadeev,⁴⁸ J. Kikuchi,⁶² D.H. Kim,⁴⁰ D.J. Kim,⁶⁵ E. Kim,⁵⁴ E. Kinney,¹¹ Á. Kiss,¹⁶ E. Kistenev,⁶ A. Kiyomichi,⁴⁹ J. Klay,³⁴ C. Klein-Boesing,³⁹ L. Kochenda,⁴⁸ V. Kochetkov,²¹ B. Komkov,⁴⁸ M. Konno,⁶⁰ D. Kotchetkov,⁷ A. Kozlov,⁶³ A. Král,¹³ A. Kravitz,¹² J. Kubart,^{8,24} G.J. Kunde,³⁵ N. Kurihara,¹⁰ K. Kurita,^{49,51} M.J. Kweon,²⁹ Y. Kwon,^{65,58} G.S. Kyle,⁴³ R. Lacey,⁵⁵ Y.S. Lai,¹² J.G. Lajoie,²⁵ A. Lebedev,²⁵ D.M. Lee,³⁵ M.K. Lee,⁶⁵ T. Lee,⁵⁴ M.J. Leitch,³⁵ M.A.L. Leite,⁵³ B. Lenzi,⁵³ X. Li,⁹ T. Liška,¹³ A. Litvinenko,²⁷ M.X. Liu,³⁵ B. Love,⁶¹ D. Lynch,⁶ C.F. Maguire,⁶¹ Y.I. Makdisi,⁵ A. Malakhov,²⁷ M.D. Malik,⁴² V.I. Manko,³⁰ Y. Mao,^{47,49} L. Mašek,^{8,24} H. Masui,⁶⁰ F. Matathias,¹² M. McCumber,⁵⁶ P.L. McGaughey,³⁵ D. McGlinchey,¹¹ Y. Miake,⁶⁰ P. Mikeš,^{8,24} K. Miki,⁶⁰ T.E. Miller,⁶¹ A. Milov,⁵⁶ S. Mioduszewski,⁶ M. Mishra,³ J.T. Mitchell,⁶ M. Mitrovski,⁵⁵ A. Morreale,⁷ D.P. Morrison,^{6,†} T.V. Moukhanova,³⁰ D. Mukhopadhyay,⁶¹ J. Murata,^{49,51} S. Nagamiya,²⁸ Y. Nagata,⁶⁰ J.L. Nagle,^{11,‡} M. Naglis,⁶³ I. Nakagawa,^{49,50} Y. Nakamiya,²⁰ T. Nakamura,²⁰ K. Nakano,^{49,59} J. Newby,³⁴ M. Nguyen,⁵⁶ B.E. Norman,³⁵ R. Nouicer,⁶ A.S. Nyanin,³⁰ E. O'Brien,⁶ S.X. Oda,¹⁰ C.A. Ogilvie,²⁵ H. Ohnishi,⁴⁹ M. Oka,⁶⁰ K. Okada,⁵⁰ O.O. Omiwade,¹ A. Oskarsson,³⁷ M. Ouchida,²⁰ K. Ozawa,¹⁰ R. Pak,⁶ D. Pal,⁶¹ A.P.T. Palounek,³⁵ V. Pantuev,^{23,56} V. Papavassiliou,⁴³ J. Park,⁵⁴ W.J. Park,²⁹ S.F. Pate,⁴³ H. Pei,²⁵ J.-C. Peng,²² H. Pereira,¹⁴ V. Peresedov,²⁷ D.Yu. Peressounko,³⁰ C. Pinkenburg,⁶ M.L. Purschke,⁶ A.K. Purwar,³⁵ H. Qu,¹⁹ J. Rak,⁴² A. Rakotozafindrabe,³² I. Ravinovich,⁶³ K.F. Read,^{45,58} S. Rembeczki,¹⁷ M. Reuter,⁵⁶ K. Reygers,³⁹ V. Riabov,⁴⁸ Y. Riabov,⁴⁸ G. Roche,³⁶ A. Romana,^{32,*} M. Rosati,²⁵ S.S.E. Rosendahl,³⁷ P. Rosnet,³⁶ P. Rukoyatkin,²⁷ V.L. Rykov,⁴⁹ B. Sahlmueller,^{39,56} N. Saito,^{31,49,50} T. Sakaguchi,⁶ S. Sakai,⁶⁰ H. Sakata,²⁰ V. Samsonov,⁴⁸ S. Sato,^{26,28} S. Sawada,²⁸ J. Seele,¹¹ R. Seidl,²² V. Semenov,²¹ R. Seto,⁷ D. Sharma,⁶³ I. Shein,²¹ A. Shevel,^{48,55} T.-A. Shibata,^{49,59} K. Shigaki,²⁰ M. Shimomura,⁶⁰ K. Shoji,^{31,49} A. Sickles,⁵⁶ C.L. Silva,⁵³ D. Silvermyr,⁴⁵ C. Silvestre,¹⁴ K.S. Sim,²⁹ C.P. Singh,³ V. Singh,³ S. Skutnik,²⁵ M. Slunečka,^{8,27} A. Soldatov,²¹ R.A. Soltz,³⁴ W.E. Sondheim,³⁵ S.P. Sorensen,⁵⁸ I.V. Sourikova,⁶ F. Staley,¹⁴ P.W. Stankus,⁴⁵ E. Stenlund,³⁷ M. Stepanov,⁴³ A. Ster,⁶⁴ S.P. Stoll,⁶ T. Sugitate,²⁰ C. Suire,⁴⁶ J. Sziklai,⁶⁴ T. Tabaru,⁵⁰ S. Takagi,⁶⁰ E.M. Takagui,⁵³ A. Taketani,^{49,50} Y. Tanaka,⁴¹ K. Tanida,^{49,50,54} M.J. Tannenbaum,⁶ A. Taranenko,⁵⁵ P. Tarján,¹⁵ T.L. Thomas,⁴² M. Togawa,^{31,49} A. Toia,⁵⁶ J. Tojo,⁴⁹ L. Tomášek,²⁴ H. Torii,⁴⁹ R.S. Towell,¹ V.-N. Tram,³² I. Tserruya,⁶³ Y. Tsuchimoto,²⁰ C. Vale,²⁵ H. Valle,⁶¹ H.W. van Hecke,³⁵ J. Velkovska,⁶¹ R. Vértesi,¹⁵ A.A. Vinogradov,³⁰ M. Virius,¹³ V. Vrba,²⁴ E. Vznuzdaev,⁴⁸ M. Wagner,^{31,49} D. Walker,⁵⁶ X.R. Wang,⁴³ Y. Watanabe,^{49,50} J. Wessels,³⁹ S.N. White,⁶ D. Winter,¹² C.L. Woody,⁶ M. Wysocki,¹¹ W. Xie,⁵⁰ Y.L. Yamaguchi,⁶² A. Yanovich,²¹ Z. Yasin,⁷ J. Ying,¹⁹ S. Yokkaichi,^{49,50} G.R. Young,⁴⁵ I. Younus,^{33,42}

I.E. Yushmanov,³⁰ W.A. Zajc,¹² O. Zaudtke,³⁹ C. Zhang,⁴⁵ S. Zhou,⁹ J. Zimányi,^{64,*} and L. Zolin²⁷

(PHENIX Collaboration)

- ¹Abilene Christian University, Abilene, Texas 79699, USA
²Department of Physics, Augustana College, Sioux Falls, South Dakota 57197, USA
³Department of Physics, Banaras Hindu University, Varanasi 221005, India
⁴Baruch College, City University of New York, New York, New York, 10010 USA
⁵Collider-Accelerator Department, Brookhaven National Laboratory, Upton, New York 11973-5000, USA
⁶Brookhaven National Laboratory, Upton, New York 11973-5000, USA
⁷University of California - Riverside, Riverside, California 92521, USA
⁸Charles University, Ovocný trh 5, Praha 1, 116 36, Prague, Czech Republic
⁹Science and Technology on Nuclear Data Laboratory, China Institute of Atomic Energy, Beijing 102413, P. R. China
¹⁰Center for Nuclear Study, Graduate School of Science, University of Tokyo, 7-3-1 Hongo, Bunkyo, Tokyo 113-0033, Japan
¹¹University of Colorado, Boulder, Colorado 80309, USA
¹²Columbia University, New York, New York 10027 and Nevis Laboratories, Irvington, New York 10533, USA
¹³Czech Technical University, Zikova 4, 166 36 Prague 6, Czech Republic
¹⁴Dapnia, CEA Saclay, F-91191, Gif-sur-Yvette, France
¹⁵Debrecen University, H-4010 Debrecen, Egyetem tér 1, Hungary
¹⁶ELTE, Eötvös Loránd University, H - 1117 Budapest, Pázmány P. s. 1/A, Hungary
¹⁷Florida Institute of Technology, Melbourne, Florida 32901, USA
¹⁸Florida State University, Tallahassee, Florida 32306, USA
¹⁹Georgia State University, Atlanta, Georgia 30303, USA
²⁰Hiroshima University, Kagamiyama, Higashi-Hiroshima 739-8526, Japan
²¹IHEP Protvino, State Research Center of Russian Federation, Institute for High Energy Physics, Protvino, 142281, Russia
²²University of Illinois at Urbana-Champaign, Urbana, Illinois 61801, USA
²³Institute for Nuclear Research of the Russian Academy of Sciences, prospekt 60%-letiya Oktyabrya 7a, Moscow 117312, Russia
²⁴Institute of Physics, Academy of Sciences of the Czech Republic, Na Slovance 2, 182 21 Prague 8, Czech Republic
²⁵Iowa State University, Ames, Iowa 50011, USA
²⁶Advanced Science Research Center, Japan Atomic Energy Agency, 2-4 Shirakata Shirane, Tokai-mura, Naka-gun, Ibaraki-ken 319-1195, Japan
²⁷Joint Institute for Nuclear Research, 141980 Dubna, Moscow Region, Russia
²⁸KEK, High Energy Accelerator Research Organization, Tsukuba, Ibaraki 305-0801, Japan
²⁹Korea University, Seoul, 136-701, Korea
³⁰Russian Research Center “Kurchatov Institute”, Moscow, 123098 Russia
³¹Kyoto University, Kyoto 606-8502, Japan
³²Laboratoire Leprince-Ringuet, Ecole Polytechnique, CNRS-IN2P3, Route de Saclay, F-91128, Palaiseau, France
³³Physics Department, Lahore University of Management Sciences, Lahore, Pakistan
³⁴Lawrence Livermore National Laboratory, Livermore, California 94550, USA
³⁵Los Alamos National Laboratory, Los Alamos, New Mexico 87545, USA
³⁶LPC, Université Blaise Pascal, CNRS-IN2P3, Clermont-Fd, 63177 Aubiere Cedex, France
³⁷Department of Physics, Lund University, Box 118, SE-221 00 Lund, Sweden
³⁸Department of Physics, University of Michigan, Ann Arbor, Michigan 48109-1040, USA
³⁹Institut für Kernphysik, University of Muenster, D-48149 Muenster, Germany
⁴⁰Myongji University, Yongin, Kyonggido 449-728, Korea
⁴¹Nagasaki Institute of Applied Science, Nagasaki-shi, Nagasaki 851-0193, Japan
⁴²University of New Mexico, Albuquerque, New Mexico 87131, USA
⁴³New Mexico State University, Las Cruces, New Mexico 88003, USA
⁴⁴Department of Physics and Astronomy, Ohio University, Athens, Ohio 45701, USA
⁴⁵Oak Ridge National Laboratory, Oak Ridge, Tennessee 37831, USA
⁴⁶IPN-Orsay, Université Paris Sud, CNRS-IN2P3, BP1, F-91406, Orsay, France
⁴⁷Peking University, Beijing 100871, P. R. China
⁴⁸PNPI, Petersburg Nuclear Physics Institute, Gatchina, Leningrad region, 188300, Russia
⁴⁹RIKEN Nishina Center for Accelerator-Based Science, Wako, Saitama 351-0198, Japan
⁵⁰RIKEN BNL Research Center, Brookhaven National Laboratory, Upton, New York 11973-5000, USA
⁵¹Physics Department, Rikkyo University, 3-34-1 Nishi-Ikebukuro, Toshima, Tokyo 171-8501, Japan
⁵²Saint Petersburg State Polytechnic University, St. Petersburg, 195251 Russia
⁵³Universidade de São Paulo, Instituto de Física, Caixa Postal 66318, São Paulo CEP05315-970, Brazil
⁵⁴Seoul National University, Seoul, Korea
⁵⁵Chemistry Department, Stony Brook University, SUNY, Stony Brook, New York 11794-3400, USA
⁵⁶Department of Physics and Astronomy, Stony Brook University, SUNY, Stony Brook, New York 11794-3400, USA
⁵⁷SUBATECH (Ecole des Mines de Nantes, CNRS-IN2P3, Université de Nantes) BP 20722 - 44307, Nantes, France
⁵⁸University of Tennessee, Knoxville, Tennessee 37996, USA
⁵⁹Department of Physics, Tokyo Institute of Technology, Oh-okayama, Meguro, Tokyo 152-8551, Japan
⁶⁰Institute of Physics, University of Tsukuba, Tsukuba, Ibaraki 305, Japan

⁶¹*Vanderbilt University, Nashville, Tennessee 37235, USA*

⁶²*Waseda University, Advanced Research Institute for Science and Engineering, 17 Kikui-cho, Shinjuku-ku, Tokyo 162-0044, Japan*

⁶³*Weizmann Institute, Rehovot 76100, Israel*

⁶⁴*Institute for Particle and Nuclear Physics, Wigner Research Centre for Physics, Hungarian Academy of Sciences (Wigner RCP, RMKI) H-1525 Budapest 114, POBox 49, Budapest, Hungary*

⁶⁵*Yonsei University, IPAP, Seoul 120%-749, Korea*

(Dated: August 14, 2019)

The PHENIX Collaboration at the Relativistic Heavy Ion Collider has measured open heavy flavor production in Cu+Cu collisions at $\sqrt{s_{NN}}=200$ GeV through the measurement of electrons at midrapidity that originate from semileptonic decays of charm and bottom hadrons. In peripheral Cu+Cu collisions an enhanced production of electrons is observed relative to $p+p$ collisions scaled by the number of binary collisions. In the transverse momentum range from 1 to 5 GeV/ c the nuclear modification factor is $R_{AA}\sim 1.4$. As the system size increases to more central Cu+Cu collisions, the enhancement gradually disappears and turns into a suppression. For $p_T > 3$ GeV/ c , the suppression reaches $R_{AA}\sim 0.8$ in the most central collisions. The p_T and centrality dependence of R_{AA} in Cu+Cu collisions agree quantitatively with R_{AA} in $d+Au$ and Au+Au collisions, if compared at similar number of participating nucleons (N_{part}).

PACS numbers: 25.75.Cj

I. INTRODUCTION

Studies of the hot matter formed in ultrarelativistic heavy ion collisions, such as those produced at the Relativistic Heavy Ion Collider (RHIC), require experimental probes, like heavy quarks (charm and bottom), that are produced during the collisions. The temperature of the matter produced in $A+A$ collisions [1, 2] is much less than the heavy quark masses ($m_c\sim 1.3$ GeV, $m_b\sim 4.2$ GeV). Thus charm and bottom quarks will only be produced in the initial stage of the collision, rather than through thermal excitation or other mechanisms. Once produced, they propagate through the hot matter and their kinematic distributions are modified through interactions along their path. These medium transport effects can be studied experimentally through the spectra of decay products from hadrons with heavy quark content.

Indeed, a large suppression of high transverse momentum (p_T) electrons from semi-leptonic heavy flavor decays was discovered in Au+Au collisions at $\sqrt{s_{NN}} = 200$ GeV relative to $p+p$ collisions [3–5] in contrast to the predicted reduced suppression for heavy quarks related to light quarks due to the "dead-cone" effect [6]. It is most pronounced in central collisions, i.e. collisions with small impact parameters, and disappears in more peripheral events. The suppression of heavy flavor at high p_T was widely interpreted as evidence that heavy flavor quarks lose a significant amount of energy as they traverse hot matter [7–9]. Many effects have been taken into account in various theoretical calculations [10–15] and the data presented here will provide significant additional constraints.

There are many processes that occur in nuclear collisions which can alter the kinematic distributions of observed particles. Modifications of the parton distributions in bound nucleons will affect the production rates of particles [16]. Initial-state parton scattering and energy loss in the nucleus will also affect the observed particle spectra [17].

Until recently, the study of $p+A$ and $d+A$ collisions was considered the best way to investigate and quantify these nuclear effects, known generally as cold-nuclear-matter effects. This assumption is now challenged by recent results obtained in $p+Pb$ and $d+Au$ collisions pointing to additional phenomena that may be of hydrodynamic origin [18–21]. Therefore, careful comparison of results from $p+p$, $p+A$, $d+A$, and $A+A$, collisions is likely needed to isolate an unambiguous signature of hot nuclear matter.

Evidence for such nuclear effects was shown by PHENIX in data from $d+Au$ collisions at $\sqrt{s_{NN}} = 200$ GeV, where an enhancement of electrons from heavy flavor decays was observed relative to $p+p$ collisions [22] between $1 < p_T < 5$ GeV. The enhancement depends on centrality; as the collisions become more central the enhancement becomes more and more pronounced, in contrast to the increasing suppression observed in Au+Au collisions at the same $\sqrt{s_{NN}}$. Given these results, it is interesting to measure how this enhancement changes over to suppression as the system becomes larger. The system size can be varied by changing the colliding nuclei.

At RHIC, effects from cold and hot nuclear matter compete and their relative importance likely depends on the system size, which can be quantified through the average number of binary nucleon-nucleon collisions ($\langle N_{coll} \rangle$) or the average number of participants ($\langle N_{part} \rangle$). Using $\langle N_{coll} \rangle$, central $d+Au$ collisions show the largest enhancement at $N_{coll}\sim 15$, while central Au+Au collisions exhibit the largest suppression at $N_{coll}\sim 1000$ (see Table I). To further investigate system-size depen-

*Deceased

[†]PHENIX Co-Spokesperson: morrison@bnl.gov

[‡]PHENIX Co-Spokesperson: jamie.nagle@colorado.edu

dence, PHENIX has studied Cu+Cu collisions, also at $\sqrt{s_{NN}}=200$ GeV. The $\langle N_{\text{coll}} \rangle$ range for this intermediate-sized system overlaps with d +Au as well as Au+Au collisions and thus Cu+Cu allows access to the transition region between dominance of enhancement effects and hot-nuclear-matter suppression.

TABLE I: Values of the average number of binary collisions ($\langle N_{\text{coll}} \rangle$) and participating nucleons ($\langle N_{\text{part}} \rangle$) for d +Au, Cu+Cu, and Au+Au collisions at $\sqrt{s_{NN}} = 200$ GeV. $\langle N_{\text{part}} \rangle$ and $\langle N_{\text{coll}} \rangle$ increase with decreasing impact parameter (more central events).

Colliding species	Centrality	$\langle N_{\text{coll}} \rangle$	$\langle N_{\text{part}} \rangle$
d +Au	0%–100%	7.59 ± 0.43	9.1 ± 0.4
	0%–20%	15.06 ± 1.01	15.4 ± 1.0
	20%–40%	10.25 ± 0.70	10.6 ± 0.7
	40%–60%	6.58 ± 0.44	7.0 ± 0.6
	60%–88%	3.20 ± 0.19	3.1 ± 0.3
Cu+Cu	0%–94%	51.8 ± 5.6	34.6 ± 1.2
	0%–10%	182.7 ± 20.7	98.2 ± 2.4
	0%–20%	151.8 ± 17.1	85.9 ± 2.3
	20%–40%	61.2 ± 6.6	45.2 ± 1.7
	40%–60%	22.3 ± 2.9	21.2 ± 1.4
	60%–94%	5.1 ± 0.7	6.4 ± 0.4
Au+Au	0%–92%	257.8 ± 25.4	109.1 ± 4.1
	0%–10%	955.4 ± 93.6	352.2 ± 3.3
	10%–20%	602.6 ± 59.3	234.6 ± 4.7
	20%–40%	296.8 ± 31.1	140.4 ± 4.9
	40%–60%	90.70 ± 11.8	59.95 ± 3.6
	60%–92%	14.50 ± 4.00	14.5 ± 2.5

In this paper we present data of single electrons (we refer to electrons to mean the sum of electrons and positrons divided by two) from semi-leptonic decays of heavy flavor hadrons obtained in Cu+Cu collisions at $\sqrt{s_{NN}} = 200$ GeV. The paper is organized as follows. Section II presents the experimental setup and describes how we measure the inclusive yield of electrons and positrons. In Section III we discuss how we extract the heavy flavor contribution from the inclusive yield. The results are presented in Section IV and discussed and compared to previous results in Section V and theoretical models in Section VI. Section VII gives a summary of this work.

II. EXPERIMENTAL METHODS

Figure 1 shows the layout of the 2005 PHENIX detector. Electrons and positrons are measured using the two central spectrometer arms, each of which covers the pseudorapidity range of $|\eta| < 0.35$ with an azimuthal coverage of $\Delta\phi = \pi/2$. Charged tracks are recon-

structed radially outside of an axial magnetic field using layers of drift chambers and pad chambers. Electrons are identified by hits in the ring imaging Čerenkov counter (RICH) and by requiring a match between an energy deposit in the electromagnetic calorimeter (EMCal) and the track's momentum. The RICH uses CO₂ gas at atmospheric pressure as the Čerenkov radiator. Electrons and pions begin to radiate in the RICH at $p_T > 20$ MeV/c and $p_T > 4.9$ GeV/c, respectively. The EMCal comprises four sectors in each arm. The two lowest sectors of the east arm are lead-glass and the remaining six are lead-scintillator. The angular segmentation of the lead-scintillator (lead-glass) is $\Delta\phi \times \Delta\eta \sim 0.01 \times 0.01$ (0.008x0.008) and the energy resolution is $\delta E/E \sim 4.5\% \oplus 8.3/\sqrt{E(\text{GeV})}\%$ ($4.3\% \oplus 7.7/\sqrt{E(\text{GeV})}\%$). A bag filled with He gas at atmospheric pressure is placed between the beam pipe and drift chamber (DC) entrance window to minimize photon conversions. Detailed descriptions of the PHENIX detector subsystems can be found in [23].

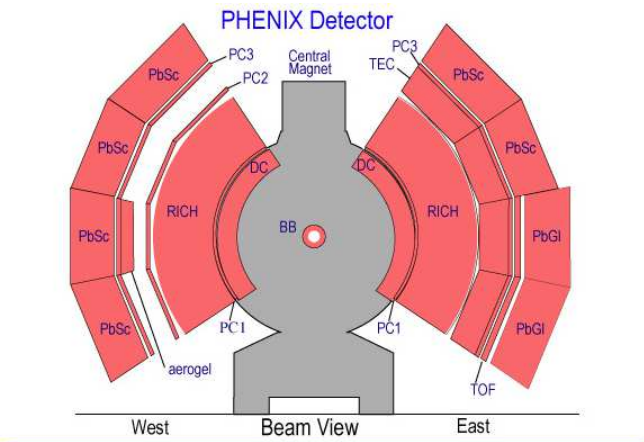


FIG. 1: (Color online) Beam view of the PHENIX central arm detector in the 2005 configuration.

For this analysis two different event samples were used. The first sample was obtained with a minimum-bias (MB) trigger, which registers all Cu+Cu collisions with a coincidence of at least one particle detected in each of the two beam-beam counters (BBC). The BBCs are located at ± 1.44 m ($3.0 < |\eta| < 3.9$) and comprise 64 Čerenkov counter modules. Only events with a vertex position within ± 20 cm of the nominal $z=0$ collision point are kept, giving a sample of 5.08×10^8 events. A second sample was collected with an additional trigger condition requiring the detection of an electron candidate in the event. This electron trigger (ERT) requires a coincidence between the EMCal and RICH detectors and provides an additional 3.3×10^9 events. For the ERT trigger, a threshold on the EMCal energy was set at approximately 1.2 GeV. In our analysis we only use electron candidates from this sample above $p_T > 3$ GeV/c, well beyond the point where the trigger reaches its maximum efficiency. The ERT trigger efficiency for electrons

over all EMCal sectors was determined to be $67\% \pm 3\%$. The largest source of inefficiency comes from dead trigger tiles.

Centrality is determined by Monte Carlo calculation of the Glauber Model [24, 25] using the measured charge deposited in the BBC. The MB collisions correspond to 0%–94% of the inelastic cross section. It is divided into centrality classes covering 0%–10%, 0%–20%, 20%–40%, 40%–60%, and 60%–94% of the centrality range (see Table I).

The analysis method used here, with some differences, is described in detail in [3]. Electron candidates start with charged tracks reconstructed by the drift chambers and pad chambers. These tracks are then identified as electrons by passing a set of electron identification cuts. First the track is projected to the RICH and at least 5 PMTs containing one registered signal are required in a disc ($r=11$ cm), with an angular size of 0.044 rad, centered at the projection point. This analysis uses a disc to reduce sensitivity to any possible mirror misalignment. The use of a tight RICH cut ensures a negligible contamination of hadrons with p_T above the RICH radiator threshold through the p_T range (<7 GeV/ c) of this analysis. The track is then projected to the EMCal and a three sigma cut is made on the difference between the projection and the center of the energy deposition.

A cut is also made on the shape of the EMCal shower, called prob, calculated from the deviation between the actual tower energy distribution and the expected distribution for an electromagnetic shower and normalized to be between 0 and 1. We require $\text{prob} > 0.01$ which has a 99% efficiency for an electromagnetic shower while rejecting a large fraction of hadrons. Finally a cut is made on the ratio of the energy deposited in the EMCal to the momentum determined by the DC, represented by E/p . An electron deposits most of its energy in the EMCal and because its mass is so small, $E \approx p$ and E/p for an electron will be close to 1. The E/p cut is made symmetrically around 1 (between 0.8 and 1.2).

Though the electron ID cuts give a good sample of electrons, in a high multiplicity environment overlap in the detectors can cause hadrons to be misidentified as electrons. The number and properties of those fake tracks reconstructed by random association can be obtained by exchanging, in software, the North and South halves of the RICH. For example, DC tracks from the South are matched with the RICH North and vice versa. After the swap, there cannot be any actual tracks, and all reconstructed ones are, by definition, fake tracks. The active area of the North and South RICH detectors are identical within $\approx 1\%$. In peripheral collisions, 3% of all tracks are mismatches, and in the central collisions that fraction rises to 22%.

A GEANT simulation of the full PHENIX detector was used to determine the extrapolation to full azimuthal acceptance and correction for electron detection efficiency. The same eID and fiducial cuts are made on the simulation output and the data. The simulated electrons were

generated flat in p_T to give sufficient statistics at high momentum, and then weighted with a realistic p_T distribution to account for momentum smearing effects due to the finite momentum resolution of the drift chamber.

III. ISOLATING THE HEAVY FLAVOR YIELD

The inclusive single electron spectrum has contributions from a multitude of sources of which heavy flavor decays is only one. Most of the electrons come from decays of light mesons (dominated by the neutral pion Dalitz decay, $\pi^0 \rightarrow \gamma e^+ e^-$) [26]. Electrons from conversions of decay photons are also significant. However, the low material design of the PHENIX detector minimizes this contribution to less than half of that from Dalitz decays. Direct photons can also be a significant contribution to the inclusive electron spectrum, either through conversions of real photons in material or manifestations of virtual photons as an $e^+ e^-$ pair. This group of electrons is collectively known as “photonic” electrons, due to their origins with either a real or virtual direct or decay photon.

The other class of electrons, known as “nonphotonic”, is dominated by the decays of open heavy flavor hadrons. The dielectron decays of the ρ , ω , and ϕ mesons contribute to the inclusive electron sample at the few percent level. Decays of quarkonia, dominated by $J/\psi \rightarrow e^+ e^-$ [27], are a significant source of nonphotonic electrons at moderate p_T . Misreconstructed electron tracks from kaon K_{e3} decays away from the collision vertex are $\sim 10\%$ of the inclusive electrons at $p_T < 1$ GeV/ c , but are negligible at higher p_T . Electron pairs produced via the Drell-Yan process contribute a negligibly small background to the heavy flavor signal. To isolate the contribution of open heavy flavor decays to the inclusive electron spectrum, these backgrounds must be determined and removed from the inclusive electron sample. The methods for isolating the open heavy flavor electron yield used in this measurement are described in detail in [3], and are summarized here for completeness.

The first method calculates a cocktail of electrons from the nonheavy flavor sources. Because the PHENIX experiment is a multipurpose detector, most of the dominant sources of single electrons have previously been measured in the same experiment. The largest background source comes from the neutral pion, both the Dalitz decay and the conversion of photons from the $\pi^0 \rightarrow \gamma\gamma$ decay. Using a parametrization of the measured π^0 p_T spectra [26] in a Monte Carlo decay generator, the p_T spectrum of daughter electrons is determined. The p_T spectra of the other light mesons that contribute to the cocktail (η , ρ , ω , η' , and ϕ) are derived from the π^0 spectrum by m_T scaling (replacing p_T in the parametrization with $\sqrt{p_T^2 + m_{meson}^2 - m_{\pi^0}^2}$) and then normalizing to the measured meson to pion ratios at high p_T . At intermediate p_T the contribution from J/ψ decays becomes

significant and the measured p_T spectra [27] are fit and used as the parent p_T spectra in the decay generator. The cocktail of nonheavy flavor electrons is subtracted from the inclusive electron sample to isolate the contribution from open heavy flavor electrons. This method works well at larger p_T where the heavy flavor contribution is significant, but suffers from large systematic uncertainties at low electron p_T , where the ratio of open heavy flavor electrons to all electrons is low.

The second method of isolating the open heavy flavor yield uses a “converter” to deliberately increase the photonic background by a well defined amount. In the standard PHENIX configuration, the number of inclusive electrons in a given p_T range N_e^{standard} can be expressed as

$$N_e^{\text{standard}} = N^\gamma + N^{\text{non-}\gamma} \quad (1)$$

where N^γ and $N^{\text{non-}\gamma}$ are the number of photonic and nonphotonic electrons in that p_T bin, respectively.

The converter is a sheet of brass, 0.25 mm thick, which has a radiation length determined to a precision of $\pm 0.25\%$. For a portion of 2005 running, the converter was wrapped around the beam pipe. This extra material increases the real photonic electron background by an amount R_γ , and reduces the nonphotonic electrons by a factor $(1 - \epsilon)$, giving an inclusive electron yield in the converter configuration $N_e^{\text{converter}}$ of

$$N_e^{\text{converter}} = R_\gamma N^\gamma + (1 - \epsilon) N^{\text{non-}\gamma} \quad (2)$$

where the factors R_γ and ϵ are determined through simulation. R_γ has a slight p_T dependence that is prevalent in the low p_T region and plateaus at a value of 2.4, and $\epsilon = 0.021 \pm 0.005$. The uncertainties on these quantities are found by varying the radiation length of the converter material in simulation by the uncertainty in the measured converter thickness.

A simultaneous solution of Eqs. 1 and 2 gives the quantity of interest $N^{\text{non-}\gamma}$. The remaining nonphotonic background electrons are subtracted following the cocktail method previously described to isolate the open heavy flavor electron contribution. Because the converter produces an undesirable background for other measurements at PHENIX, it is only installed for a relatively short amount of time. Therefore the converter method of background determination is limited by the statistics of the data sample taken with the converter installed. However, at low p_T where statistical uncertainties are relatively small, the converter method provides meaningful results. Because this region is where the cocktail method is limited by systematic uncertainties, and high p_T is where the converter method is limited by statistics, the open heavy flavor electron results are determined by the converter method at $p_T < 1 \text{ GeV}/c$, and by the cocktail method elsewhere.

As a stringent cross-check of the methods described here, the ratio of nonphotonic electrons to photonic electrons,

$$R_{\text{NP}} = \frac{N^{\text{non-}\gamma}}{N^\gamma} \quad (3)$$

are compared for the two methods (shown in Fig. 2). The gray boxes are the systematic uncertainties in determining R_{NP} from the cocktail method.

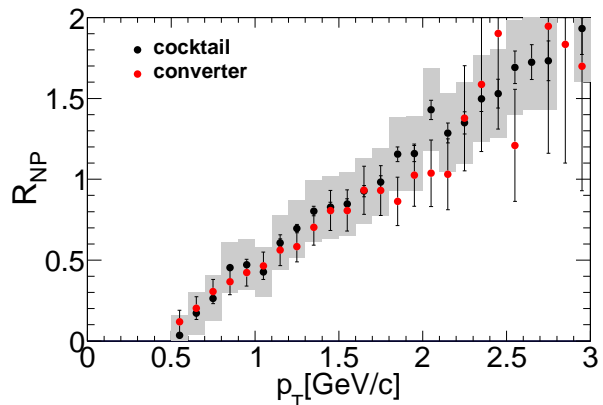


FIG. 2: (Color online) The ratio of nonphotonic to photonic electrons by the converter and cocktail methods, for MB Cu+Cu collisions.

A. Systematic Uncertainties

The systematic uncertainties on the resulting heavy flavor electron yield come from the determination of the inclusive electron yield and the uncertainty on the cocktail (converter) method. The uncertainties are explained in detail in [3] and are summarized here.

The systematic uncertainty on the inclusive yield is a combination of three parts: the uncertainty on the run group correction, electron identification, and geometric matching. For the ERT data set there is an additional uncertainty that comes from determining the trigger efficiency. The run group correction uncertainty comes from the fluctuation of the average number of electrons per event ($\langle N_e/N_{\text{evt}} \rangle$) for each run (where a run is defined as the data taken between successive starts of the PHENIX data acquisition system). The uncertainty on $\langle N_e/N_{\text{evt}} \rangle$ was found to be 1% and is assigned as the run-group-correction fluctuation. The uncertainty on identifying electrons comes from the inability to perfectly model the detector in simulation. It is estimated by repeating the acceptance*efficiency calculation for tighter and looser cuts which are then applied to inclusive yields made with the same cuts. The ratio between the standard and tight or loose cuts is found to be 6% and is taken as the systematic uncertainty. Mismatching in the detector acceptance

between simulation and data is an additional uncertainty and was found to be 4%. The ERT data set is only used in the high p_T region where the trigger efficiency is at the plateau value and so the only uncertainty is due to the determination of the trigger plateau, 2%. The total systematic uncertainty on the inclusive MB (ERT) yield is the quadrature sum of the previously discussed uncertainties and is found to be 7.3 (7.5)%.

The dominant systematic uncertainty on the cocktail comes from the uncertainty on the 2005 Cu+Cu neutral pion data [26] that is used as the input parent spectra for all of the light mesons. The pion data are moved up and down by their systematic uncertainties and refit. These new fits are then input into the decay generator and the output decay spectra become the upper and lower spread of the systematic uncertainties. The systematic uncertainty on the J/ψ spectra is done in the same manner as the pions. The rest of the light mesons are moved up and down by the uncertainty on the meson/ π^0 ratios at high p_T . The systematic uncertainty on the conversion yield is found by scaling the conversion probability up and down by 10%. This gives a conservative estimate of the uncertainty on the amount of conversion material within PHENIX. The K_{e3} is assigned a 50% uncertainty as in previous analyses. The systematic uncertainty on the cocktail is dependent on p_T and centrality but has an average value of $\sim 12\%$ for MB collisions.

The systematic uncertainty on the converter analysis comes from two sources: the already described uncertainty on the inclusive yield and the uncertainty derived from extracting a nonphotonic yield from the converter analysis. These uncertainties are independent and added in quadrature. R_γ , ϵ , and N_{inc}^C are moved up and down by their systematic uncertainties and the effect on the yield is calculated and then added in quadrature. The overall converter systematic uncertainty is found to be 8% for MB. Table II summarizes the different systematic uncertainties.

TABLE II: Systematic uncertainties on the determination of the open heavy flavor yield of electrons for MB collisions.

Run Group Correction	1%
Acceptance*Efficiency	6%
Geometric Matching	4%
Trigger Efficiency	2%
MB (ERT) Inclusive Yield	7.3% (7.5%)
Cocktail (Average)	12%
Converter	8%

IV. RESULTS FROM CU+CU COLLISIONS

The invariant yield of heavy flavor electrons is calculated as a function of p_T using the following formula:

$$\frac{1}{2\pi p_T} \frac{d^2 N^e}{dp_T dy} = \frac{1}{2\pi p_T N_{events}} \frac{N_{eHF}}{2} \frac{1}{\Delta p_T \Delta y} \frac{1}{\epsilon_{BBC} \epsilon_{eID}}, \quad (4)$$

where N_{events} is the number of events, Δp_T is the p_T bin width, Δy is the rapidity range ($|y| < 0.35$), ϵ_{BBC} is the BBC efficiency for MB (94%), ϵ_{eID} is acceptance and efficiency correction, and N_{eHF} is the calculated number of heavy flavor electrons and positrons from either the cocktail or converter method.

When plotting the invariant yield vs p_T , the average value is plotted at the bin center. However, for a steeply falling spectrum, the average value does not lie at the center of the bin. This is corrected by adjusting the average value over the bin to correspond to the value of the yield at the p_T bin center. This procedure assumes that the invariant yield as a function of p_T varies smoothly, which is a reasonable assumption.

The p_T spectra of heavy flavor electrons (e_{HF}) produced in Cu+Cu collisions at $\sqrt{s_{NN}} = 200$ GeV are shown for 5 different centralities in Fig. 3, along with a fit to the e_{HF} spectrum from $p+p$ collisions (as reported in [3]) scaled by $\langle N_{coll} \rangle$. Above $p_T = 1$ GeV/c, the spectra are taken from the cocktail method described previously, while at lower p_T the spectra are determined by the converter method.

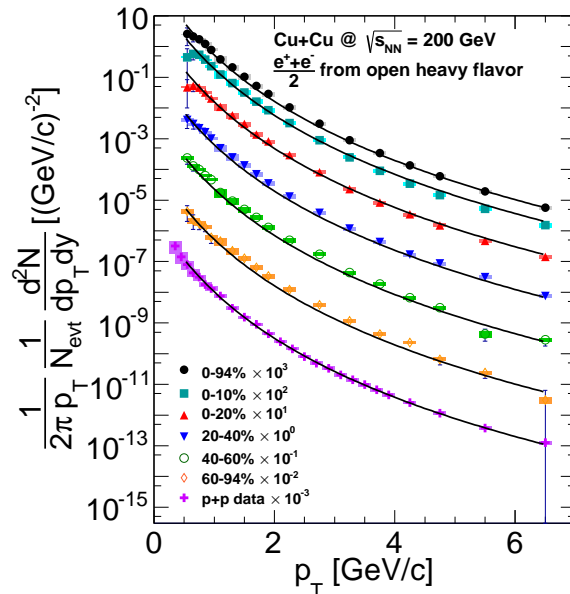


FIG. 3: (Color online) The p_T spectra of electrons from the decays of open heavy flavor hadrons produced in Cu+Cu collisions, separated by centrality. The lines are a fit to the $p+p$ data [3] scaled by $\langle N_{coll} \rangle$.

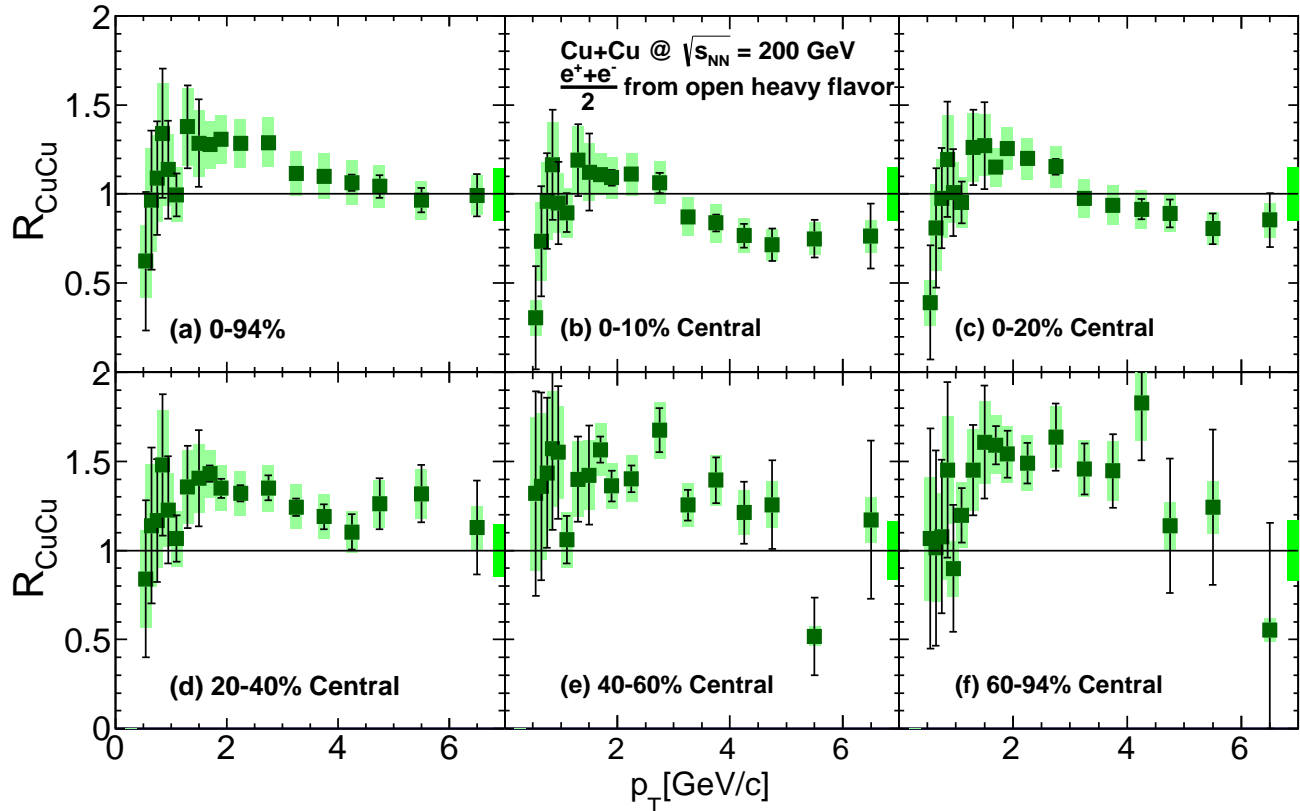


FIG. 4: (Color online) The nuclear modification factor for MB (0%–94%) and five centrality bins (0%–10%, 0%–20%, 20%–40%, 40%–60%, 60%–94%). The boxes around one are Type C global uncertainties, which include the $\langle N_{\text{coll}} \rangle$ scaling error and $p+p$ global uncertainty (9.9%) added in quadrature.

To quantify nuclear effects, the nuclear modification factor R_{AA} is calculated according to:

$$R_{AA} = \frac{dN_{A+A}^e/dp_T}{\langle N_{\text{coll}} \rangle \times dN_{p+p}^e/dp_T}, \quad (5)$$

where dN_{A+A}^e/dp_T (dN_{p+p}^e/dp_T) is the differential yield in $A+A$ ($p+p$) collisions. An R_{AA} value of one indicates that the $A+A$ data are well described by a superposition of independent $p+p$ collisions. Following [3, 22], at $p_T < 1.6 \text{ GeV}/c$, R_{AA} is calculated by dividing the Cu+Cu spectra by the $p+p$ spectra point-by-point. The statistical (systematic) uncertainties on R_{AA} in this range are the quadrature sum of the statistical (systematic) uncertainties on the Cu+Cu and $p+p$ yields in a given p_T bin.

Above $p_T = 1.6 \text{ GeV}/c$, where the $p+p$ data are well represented by the shape from fixed-order plus next-to-leading-log calculations from Ref. [28], a fit to that shape is used to represent the $p+p$ denominator. A function of the form

$$Y(p_T) = \frac{A}{(p_T + B)^n}, \quad (6)$$

is fit to these data, where $A=0.0067 \pm 0.0035 (\text{GeV}/c)^{-2}$,

$B=1.079 \pm 0.085 \text{ GeV}/c$, and $n=8.86 \pm 0.23$. Here, the statistical uncertainty on R_{AA} is determined by the statistical uncertainty on the Cu+Cu spectra. The systematic uncertainty on R_{AA} is the quadrature sum of the systematic uncertainty on the e_{HF} yield from Cu+Cu and $p+p$, and the statistical uncertainty on the fit to the $p+p$ data. The Type C global scaling uncertainty plotted around 1 is the quadrature sum of the global uncertainty on the $p+p$ spectra and the uncertainty on $\langle N_{\text{coll}} \rangle$.

Figure 4(b) shows the nuclear modification factor for the 0%–10% most central Cu+Cu collisions, in which a moderate suppression of e_{HF} is observed for $p_T > 3 \text{ GeV}/c$. This suppression is usually attributed to energy loss in the hot nuclear medium. Although this is a significant deviation from a superposition of independent $p+p$ collisions, the magnitude of suppression is smaller than what is seen in central Au+Au collisions [3, 4].

In contrast, a significant enhancement is observed in more peripheral Cu+Cu collisions, Fig. 4. To quantitatively examine the difference within the Cu+Cu system itself, the $\langle N_{\text{coll}} \rangle$ -scaled ratio of the most central to most

peripheral spectra R_{cp} , defined as

$$R_{cp} = \frac{N_{coll}^{peripheral}}{N_{coll}^{central}} \times \frac{dN_{Cu+Cu}^{central}/dp_T}{dN_{Cu+Cu}^{peripheral}/dp_T} \quad (7)$$

and is shown in Fig. 5. Most of the systematic uncertainties cancel in R_{cp} , leaving only the uncertainty on the centrality dependent cocktail and the ratio of $\langle N_{coll} \rangle$ values. A clear suppression is seen in the most central collisions relative to the most peripheral, which can be attributed to the suppression effects of the hot, dense partonic matter dominating in central collisions.

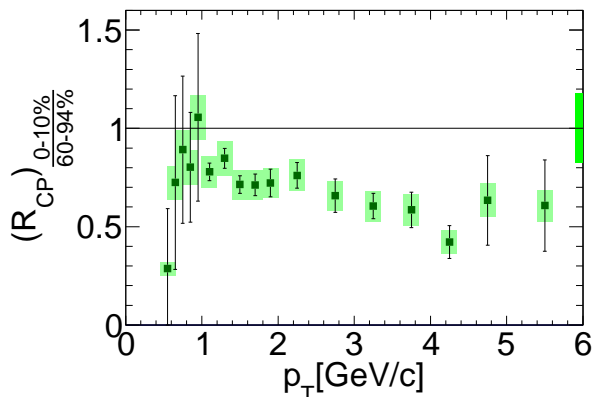


FIG. 5: (Color online) The ratio R_{cp} of the most central 0%–10% e_{HF} spectra to the most peripheral 60%–94%, scaled by $\langle N_{coll} \rangle$. Type C uncertainty is the uncertainty on the determination of $\langle N_{coll} \rangle$ for each centrality, shown as a box around 1.

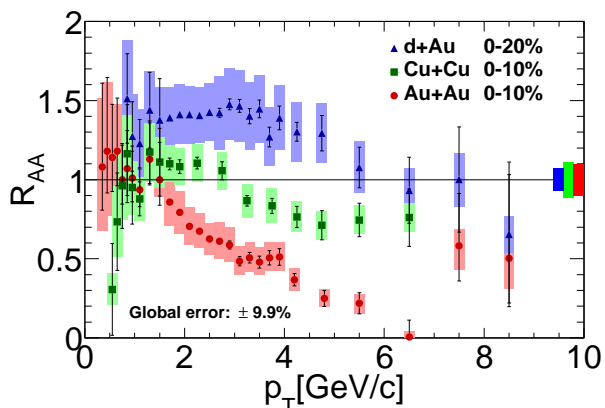


FIG. 6: (Color online) The nuclear modification factors for e_{HF} at midrapidity in central $d+Au$ [22], $Cu+Cu$, and $Au+Au$ [3] collisions at $\sqrt{s_{NN}} = 200$ GeV. The boxes around one are Type C uncertainties, which include the $\langle N_{coll} \rangle$ scaling error. The global uncertainty is that on the $p+p$ yield.

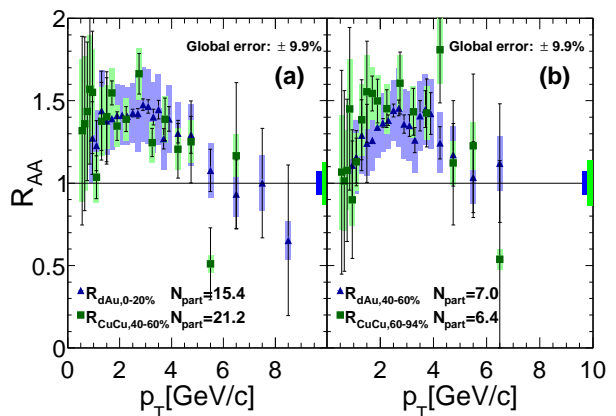


FIG. 7: (Color online) The nuclear modification factors for 0%–20% $d+Au$ [22] and 40%–60% $Cu+Cu$ collisions. Right: The nuclear modification factors for 40%–60% $d+Au$ and 60%–94% $Cu+Cu$ collisions. The boxes around one are Type C uncertainties, which include the $\langle N_{coll} \rangle$ scaling error. The global uncertainty is that on the $p+p$ yield.

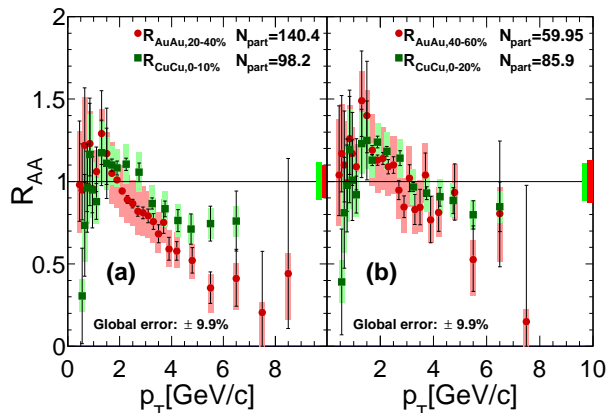


FIG. 8: (Color online) The nuclear modification factors for (a) 0%–10% $Cu+Cu$ and 20%–40% $Au+Au$ [3] collisions and (b) 0%–20% $Cu+Cu$ and 40%–60% $Au+Au$ collisions. The boxes around one are Type C uncertainties, which include the $\langle N_{coll} \rangle$ scaling error. The global uncertainty is the global uncertainty on the $p+p$ yield.

V. SYSTEM SIZE DEPENDENCE

The full extent of the system size dependence is directly illustrated by comparing the most central bins of all three systems in Fig. 6. There is a clear enhancement in central $d+Au$ collisions, which gives way to a slight suppression in central $Cu+Cu$ collisions, and finally a large suppression in the most central $Au+Au$ bin.

If results from different systems are compared in centrality bins of comparable system size the trend is similar. Here we take the number of nucleons participating in the collision, $\langle N_{part} \rangle$, as a measure of the centrality and of the size of the system. The centrality selections are the

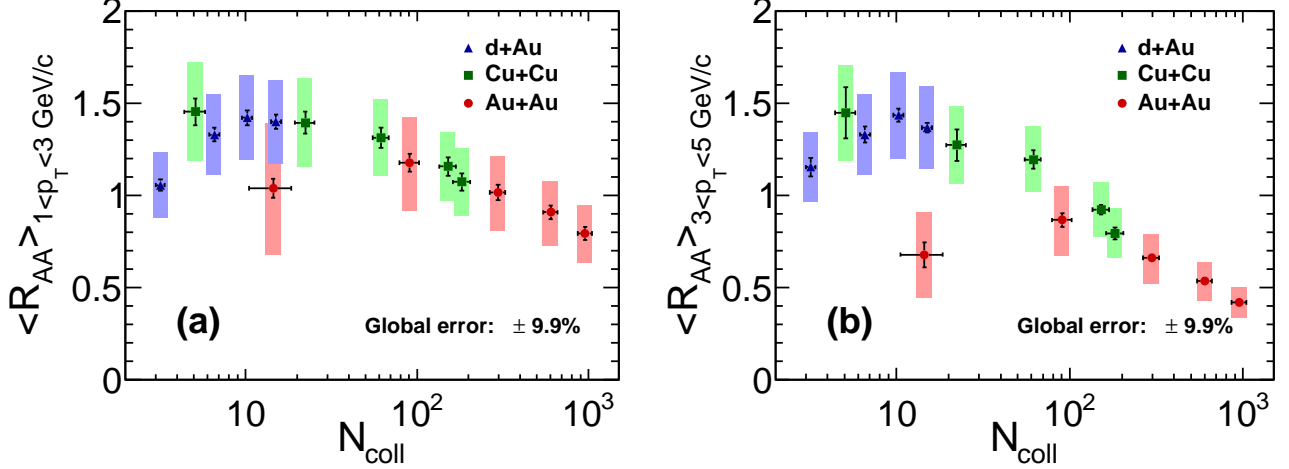


FIG. 9: (Color online) The nuclear modification factors, averaged over $1 < p_T < 3$ GeV/c (a) and $3 < p_T < 5$ GeV/c (b), for e_{HF} at midrapidity in $d+\text{Au}$ [22], $\text{Cu}+\text{Cu}$, and $\text{Au}+\text{Au}$ [3] collisions plotted as a function of $\langle N_{\text{coll}} \rangle$.

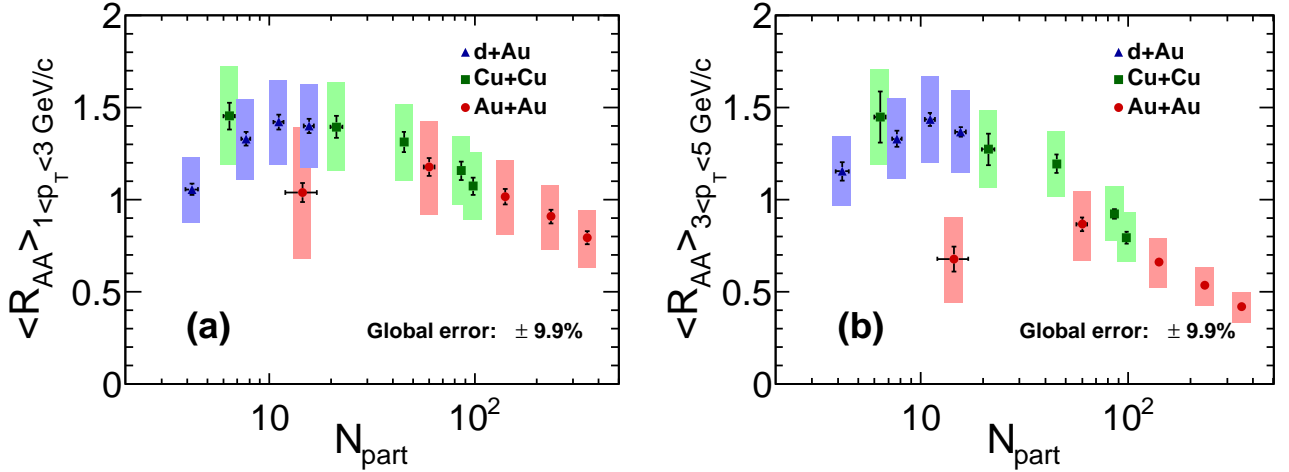


FIG. 10: (Color online) The nuclear modification factors, averaged over $1 < p_T < 3$ GeV/c (a) and $3 < p_T < 5$ GeV/c (b), for e_{HF} at midrapidity in $d+\text{Au}$ [22], $\text{Cu}+\text{Cu}$, and $\text{Au}+\text{Au}$ [3] collisions plotted as a function of $\langle N_{\text{part}} \rangle$.

same if $\langle N_{\text{coll}} \rangle$ is used as a measure of the system size instead. Figure 7 shows overlays of the R_{AA} for peripheral $\text{Cu}+\text{Cu}$ collisions with the R_{dA} for $d+\text{Au}$ collisions at a comparable value of $\langle N_{\text{part}} \rangle$. A similar enhancement is seen for the two systems.

Within the $\text{Cu}+\text{Cu}$ system, the enhancement is overtaken by suppression as the average impact parameter decreases and with it the number of collisions increases. To compare the levels of suppression in $\text{Cu}+\text{Cu}$ and $\text{Au}+\text{Au}$ collisions, the nuclear modification factors for heavy flavor electrons in centrality classes with comparable $\langle N_{\text{part}} \rangle$ values are shown in Fig. 8. Here our centrality selections do not allow for as close a match, but a similar level of modification is seen for the different systems at

similar values of $\langle N_{\text{part}} \rangle$.

Rather than comparing R_{AA} vs p_T for similar system size, one can also compare average R_{AA} values in a given p_T range as a function of $\langle N_{\text{part}} \rangle$ or $\langle N_{\text{coll}} \rangle$. The average value of the nuclear modification factor for $1 < p_T < 3$ GeV/c and $3 < p_T < 5$ GeV/c for the three collision species is shown in Figs. 9 and 10, as a function of $\langle N_{\text{coll}} \rangle$ and $\langle N_{\text{part}} \rangle$, respectively. With the exception of the most peripheral $\text{Au}+\text{Au}$ bin in the higher p_T range, a trend of increasing enhancement followed by suppression is seen among the three distinct systems, with $\text{Cu}+\text{Cu}$ showing evidence of both. This common trend suggests that the enhancement and suppression effects are dependent on the size of the colliding system and the produced

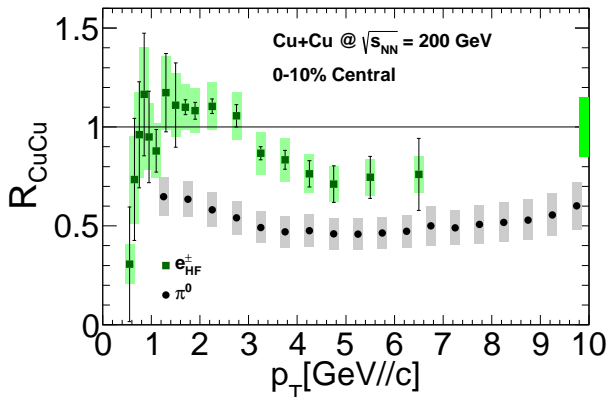


FIG. 11: (Color online) R_{AA} for π^0 and e_{HF}^+ . The boxes around one are Type C global uncertainties, which include the $\langle N_{coll} \rangle$ scaling uncertainty and $p+p$ global uncertainty.

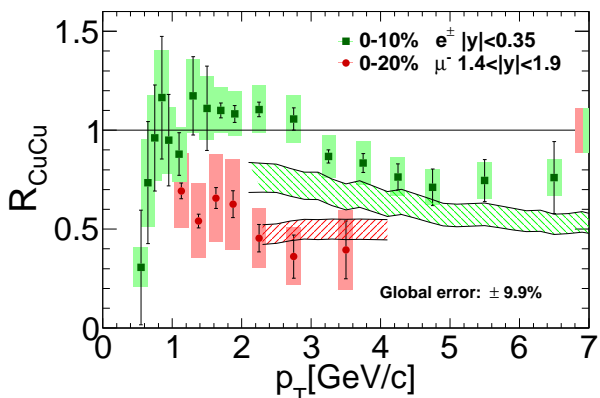


FIG. 12: (Color online) The nuclear modification factors for e_{HF}^+ at midrapidity and μ_{HF}^- at forward rapidity, for the 0%–20% most central Cu+Cu collisions. The boxes around one are Type C uncertainties from the $\langle N_{coll} \rangle$ scaling error. The global uncertainty is that on the $p+p$ yield. Model bands are calculations from [37] including partonic energy loss, energy loss from fragmentation and dissociation, and effects from nuclear matter.

medium.

VI. DISCUSSION

The heavy quark data from Cu+Cu collisions display enhancement and suppression features similar to those found in both $d+Au$ and Au+Au collisions, respectively. The enhancement seen for heavy flavor electrons in central $d+Au$ is larger than what is observed for pions and kaons at the same collision energy [29]. In central $d+Au$ collisions, a mass-dependent enhancement is observed for identified pions, kaons, and protons [30]. The proton spectra show the largest enhancement and reach an R_{dA} of ~ 1.5 at $p_T = 3 \text{ GeV}/c$ in MB $d+Au$ collisions.

This hardening of hadron spectra in nuclear collisions compared to $p+p$ collisions is known as the ‘‘Cronin effect’’ [31] and is used generically for $R_{AA} > 1$ observations.

Early explanations of the mechanism behind the Cronin effect relied on k_T boosts to partons via scattering in the nucleus before the hard scattering and subsequent fragmentation [32]; however, this hypothesis does not explain the observed mass dependence, because the k_T transverse momentum kicks in the nucleus presumably occur before hadronization and therefore could not preferentially boost protons more than pions. An alternative scenario involving recombination of soft partons in the hadronization process naturally gives a difference between meson and baryon enhancement [33, 34], but it is not immediately clear what effect this has on heavy flavor electrons, which are from a mixture of charm and bottom meson and baryon decays (though most are from mesons). The baryon enhancement observed in $d+Au$ and $A+A$ collisions at RHIC can also suppress e_{HF} production at moderate p_T , because charmed baryons have a smaller branching ratio to electrons than charmed mesons [35]; however, currently no measurements of charmed baryons at RHIC energies exist to confirm any changes in the charmed hadron chemistry.

Charm and bottom production at midrapidity is dominated by gluon fusion and samples nuclear x -values of $\sim 10^{-2}$, where modification of the gluon PDF may be significant in central collisions. Because the observed enhancement occurs in peripheral Cu+Cu collisions with a large average impact parameter, where the spatially-dependent nuclear PDF is expected to have minimal changes from the free-nucleon PDF [36], this may suggest that gluon modification is not the dominant effect at midrapidity. Parton energy loss in the nucleus may also affect heavy flavor production in nuclear collisions [17]. These effects are also expected to occur in the initial stages of central nuclear collisions, prior to the formation of the hot nuclear medium. The observed enhancement is theoretically unexplained.

Several mechanisms have been put forth to explain the large e_{HF} suppression in Au+Au collisions (shown in Fig. 8) when it was found that radiative energy loss alone was not sufficient to reproduce the suppression [38]. Recent models involving collisional energy loss and energy loss through in-medium dissociation of heavy flavor mesons in addition to gluon radiation have proven more successful at describing the Au+Au data [13, 14, 39–41]. Fragmentation and dissociation have recently been used to describe the suppression of the quarkonia yield in Au+Au collisions and could also be applied to the heavy-light bound states of the D and B meson [42]. These effects are sensitive to the formation times of the mesons and the hot nuclear medium.

It was originally thought that heavy quarks would exhibit less suppression than light quarks in a deconfined medium, due to a suppression of small-angle gluon radiation known as the ‘‘dead cone’’ effect [6]. The e_{HF} and π^0

R_{AA} for central Cu+Cu collisions are shown in Fig. 11. The heavy flavor electrons seem to approach the level of suppression of the neutral pions, though the electron p_T range is limited. While this may suggest a difference in energy loss for light and heavy quarks, the peripheral π^0 data show none of the enhancement that is present for heavy flavor. Because the nuclear effects are expected to be present in the initial state of central collisions, the different level of suppression for e_{HF} and π^0 may indicate that the initial state effects on light and heavy quarks are different. A similar difference is also observed in d +Au collisions, where the e_{HF} show significant enhancement while the π^0 does not.

Previous PHENIX measurements at forward rapidity ($1.4 < y < 1.9$) showed a significant suppression of heavy flavor muons (μ_{HF}) in central Cu+Cu collisions [43]. The magnitude of this suppression at forward rapidity in Cu+Cu (shown in Fig. 12) is comparable to the suppression of e_{HF} in central Au+Au collisions at midrapidity. This observation is difficult to reconcile with explanations of heavy flavor suppression that depend solely on energy loss in the hot nuclear medium, because the energy density of the matter created in central Au+Au collisions is expected to be larger than in Cu+Cu collisions [43, 44]. Because open heavy flavor is significantly more suppressed at forward rapidity than at midrapidity in Cu+Cu, additional nuclear effects, such as gluon shadowing at low x or partonic energy loss in the nucleus, may be significant. Suppression through shadowing effects may also be relevant to heavy flavor production at midrapidity at the Large Hadron Collider [45], because the $\sqrt{s_{NN}}$ is higher than at RHIC and probes a lower x -range within the nucleus at midrapidity.

The heavy flavor electrons and muons are compared in Fig. 12 to a theoretical prediction that combines the effects of partonic energy loss, energy loss from fragmentation and dissociation, and includes nuclear matter effects such as shadowing and Cronin enhancement due to parton scattering in the nucleus [37]. While consistent within uncertainties, the model predicts more suppression for heavy flavor electrons than seen in the data. The B mesons are heavier and so dissociation is the dominant contribution to the energy loss for the entire p_T range at RHIC in this model. On the other hand, with its lighter mass, the D meson transitions at $p_T \sim 5$ GeV to the traditional partonic energy loss. However, it is critical to test models against the full range of system sizes to have confidence in the underlying model physics and so calculations are needed for d +Au and peripheral Cu+Cu.

VII. SUMMARY AND CONCLUSIONS

The Cu+Cu data presented here build a bridge between the enhancement observed in d +Au collisions and the suppression found in Au+Au. We find that for electrons between 1 and 3 GeV/ c the variation in R_{AA} is common as a function of $\langle N_{part} \rangle$ or $\langle N_{coll} \rangle$ in d +Au,

Cu+Cu, and Au+Au. For electrons between 3–5 GeV/ c this relation also holds with the exception of the most peripheral Au+Au. Peripheral collisions of Cu nuclei display an enhancement of open heavy flavor at moderate p_T that is consistent with the enhancement observed in d +Au collisions at similar values of $\langle N_{coll} \rangle$ and $\langle N_{part} \rangle$, which suggests significant effects on heavy quark production are present in the initial state of heavy ion collisions. In central Cu+Cu collisions, open heavy flavor at midrapidity is moderately suppressed when compared to a superposition of independent p + p collisions, and significantly suppressed compared to peripheral Cu+Cu collisions. The nuclear modification factor R_{AA} displays a suppression that is consistent with that seen in semi-peripheral Au+Au collisions with a similar system size, suggesting that the suppressing effects from hot nuclear matter are becoming dominant.

While partonic energy loss in medium alone does not describe either the Cu+Cu or Au+Au e_{HF} data, a model which incorporates initial state gluon shadowing, parton scattering and energy loss in nuclear matter, followed by dissociative energy loss in the hot medium, gives a reasonable description of central Cu+Cu open heavy flavor data at both midrapidity and forward rapidity. Models that describe central Au+Au should also be tested against the Cu+Cu and d +Au data. A number of different effects must be balanced to describe the data, which demonstrates the complicated interplay of effects from nuclear matter and those from the hot medium in heavy ion collisions.

ACKNOWLEDGMENTS

We thank the staff of the Collider-Accelerator and Physics Departments at Brookhaven National Laboratory and the staff of the other PHENIX participating institutions for their vital contributions. We acknowledge support from the Office of Nuclear Physics in the Office of Science of the Department of Energy, the National Science Foundation, Abilene Christian University Research Council, Research Foundation of SUNY, and Dean of the College of Arts and Sciences, Vanderbilt University (U.S.A), Ministry of Education, Culture, Sports, Science, and Technology and the Japan Society for the Promotion of Science (Japan), Conselho Nacional de Desenvolvimento Científico e Tecnológico and Fundação de Amparo à Pesquisa do Estado de São Paulo (Brazil), Natural Science Foundation of China (P. R. China), Ministry of Education, Youth and Sports (Czech Republic), Centre National de la Recherche Scientifique, Commissariat à l'Énergie Atomique, and Institut National de Physique Nucléaire et de Physique des Particules (France), Bundesministerium für Bildung und Forschung, Deutscher Akademischer Austausch Dienst, and Alexander von Humboldt Stiftung (Germany), Hungarian National Science Fund, OTKA (Hungary), Department of Atomic Energy (India), Israel Science Foundation (Is-

rael), National Research Foundation and WCU program of the Ministry Education Science and Technology (Korea), Physics Department, Lahore University of Management Sciences (Pakistan), Ministry of Education and Science, Russian Academy of Sciences, Federal Agency of

Atomic Energy (Russia), VR and Wallenberg Foundation (Sweden), the U.S. Civilian Research and Development Foundation for the Independent States of the Former Soviet Union, the US-Hungarian NSF-OTKA-MTA, and the US-Israel Binational Science Foundation.

-
- [1] F. Karsch, Lect. Notes Phys. **583**, 209 (2002).
- [2] A. Adare *et al.* (PHENIX Collaboration), Phys. Rev. Lett. **104**, 132301 (2010).
- [3] A. Adare *et al.* (PHENIX Collaboration), Phys. Rev. C **84**, 044905 (2011).
- [4] A. Adare *et al.* (PHENIX Collaboration), Phys. Rev. Lett. **98**, 172301 (2007).
- [5] A. Adare *et al.* (PHENIX Collaboration), Phys. Rev. Lett. **97**, 252002 (2006).
- [6] Y. L. Dokshitzer and D. Kharzeev, Phys. Lett. B **519**, 199 (2001).
- [7] G. D. Moore and D. Teaney, Phys. Rev. C **71**, 064904 (2005).
- [8] P. B. Gossiaux and J. Aichelin, Phys. Rev. C **78**, 014904 (2008).
- [9] H. van Hees, V. Greco, and R. Rapp, Phys. Rev. C **73**, 034913 (2006).
- [10] P. B. Gossiaux, R. Bierkanndt, and J. Aichelin, Phys. Rev. C **79**, 044906 (2009).
- [11] P. B. Gossiaux and J. Aichelin, J. Phys. G **36**, 064028 (2009).
- [12] M. G. Mustafa, Phys. Rev. C **72**, 014905 (2005).
- [13] S. Wicks, W. Horowitz, M. Djordjevic, and M. Gyulassy, Nucl. Phys. A **783**, 493 (2007).
- [14] A. Adil and I. Vitev, Phys. Lett. B **649**, 139 (2007).
- [15] P. Sorensen and X. Dong, Phys. Rev. C **74**, 024902 (2006).
- [16] K. J. Eskola, H. Paukkunen, and C. A. Salgado, J. High Energy Phys. **04** (2009) 065.
- [17] I. Vitev, Phys. Rev. C **75**, 064906 (2007).
- [18] A. Adare *et al.* (PHENIX Collaboration), arXiv:1303.1794 and to be published.
- [19] S. Chatrchyan *et al.*, Phys. Lett. B **718**, 795 (2013).
- [20] B. Abelev *et al.* (ALICE Collaboration), Phys. Lett. B **719**, 29 (2013).
- [21] G. Aad *et al.* (ATLAS Collaboration), Phys. Rev. Lett. **110**, 182302 (2013).
- [22] A. Adare *et al.* (PHENIX Collaboration), Phys. Rev. Lett. **109**, 242301 (2012).
- [23] K. Adcox *et al.* (PHENIX Collaboration), Nucl. Instrum. Methods A **499**, 469 (2003).
- [24] M. L. Miller, K. Reygers, S. J. Sanders, and P. Steinberg, Ann. Rev. Nucl. Part. Sci. **57**, 205 (2007).
- [25] R. Glauber and G. Matthiae, Nucl. Phys. B **21**, 135 (1970).
- [26] A. Adare *et al.* (PHENIX Collaboration), Phys. Rev. Lett. **101**, 162301 (2008).
- [27] A. Adare *et al.* (PHENIX Collaboration), Phys. Rev. Lett. **101**, 122301 (2008).
- [28] M. Cacciari, P. Nason, and R. Vogt, Phys. Rev. Lett. **95**, 122001 (2005).
- [29] S. S. Adler *et al.* (PHENIX Collaboration), Phys. Rev. Lett. **98**, 172302 (2007).
- [30] A. Adare *et al.* (PHENIX Collaboration), Phys. Rev. C **88**, 024906 (2013).
- [31] J. W. Cronin, H. J. Frisch, M. J. Shochet, J. P. Boymond, P. A. Piroué, and R. L. Sumner, Phys. Rev. D **11**, 3105 (1975).
- [32] A. Accardi, arXiv:hep-ph/0212148.
- [33] R. C. Hwa and C. B. Yang, Phys. Rev. C **70**, 024905 (2004).
- [34] R. C. Hwa and C. B. Yang, Phys. Rev. Lett. **93**, 082302 (2004).
- [35] P. Sorensen and X. Dong, Phys. Rev. C **74**, 024902 (2006).
- [36] I. Helenius, K. J. Eskola, H. Honkanen, and C. A. Salgado, arXiv:1205.5359.
- [37] R. Sharma, I. Vitev, and B.-W. Zhang, Phys. Rev. C **80**, 054902 (2009).
- [38] S. Wicks, W. Horowitz, M. Djordjevic, and M. Gyulassy, Nucl. Phys. A **784**, 426 (2007).
- [39] B. W. Zhang, E. Wang, and X. N. Wang, Phys. Rev. Lett. **93**, 072301 (2004).
- [40] F. Dominguez and B. Wu, Nucl. Phys. A **818**, 246 (2009).
- [41] F. Dominguez, C. Marquet, and B. Wu, Nucl. Phys. A **823**, 99 (2009).
- [42] C.-Y. Wong, Phys. Rev. C **72**, 034906 (2005).
- [43] A. Adare *et al.* (PHENIX Collaboration), Phys. Rev. C **86**, 024909 (2012).
- [44] J. D. Bjorken, Phys. Rev. D **27**, 140 (1983).
- [45] B. Abelev *et al.* (ALICE Collaboration), Phys. Rev. D **86**, 112007 (2012).